Engenharia Agrícola
ISSN: 1809-4430 (online)
www.engenhariaagricola.org.br | www.scielo.br/j/eagri

Technical Paper
DOI: http://dx.doi.org/10.1590/1809-4430-Eng.Agric.v45e20240045/2025

INFLUENCE OF THE PARAMETERS OF A FORAGE CONDITIONING ROLL ON THE AIRFLOW FIELD

Qingmiao Xiang[1], Tianlin Zuo[1], Bei Wu[1*,2], Zhuo Li[1], Huaiyuan Qian[1], Tianci Huang[1]

[1*]Corresponding author. College of Mechanical and Electrical Engineering, Hunan Agricultural University, Changsha, China.
E-mail: wubei@hunau.edu.cn | ORCID ID: https://orcid.org/0009-0006-2690-9441

KEYWORDS

mower conditioner, conditioning roll, CFD, airflow field, numerical simulation.

ABSTRACT

The influence of the airflow field around the conditioning roll of a mower conditioner on the forage harvesting process cannot be ignored. Full factorial simulation tests of the airflow field of a single conditioning roll and double conditioning roll were carried out, respectively, by taking the roll type, roll rotational velocity, and roll clearance as factors. The results show that the average airflow velocity around the conditioning rolls has a linear positive correlation with the roll velocity and an exponential negative correlation with the distance from the centre of the conditioning rolls in the single roll case. In the case of double rolls, the airflow around the conditioning rolls increase with the velocity of the rolls and decrease with the increase of the clearance between the rolls. The results of the field verification test show that, compared with the measured values for the prototype, the average error of the average velocity of the airflow around the single roll, predicted by the regression model, is 6.35%. The average error of the predicted velocity of the back-feeding airflow of the double roll is 5.86%. The results are reliable and could provide a reference for the optimised design of the conditioning roll.

INTRODUCTION

Alfalfa is known as the "King of Forages" and should be conditioned at point of harvest (Blain et al., 2023; Feng et al., 2022; Li et al., 2019). Alfalfa stems are cracked and the wax layer of the stem is destroyed by the mower conditioner. To ensure that the stem and leaves are dried at the same time, the alfalfa drying time is shortened in the field, avoiding the shedding of leaves due to over-drying in the subsequent mechanical operations to improve the quality of alfalfa hay products (El-Baily, 2022; Liu et al., 2022; Zhortuylov et al., 2019; Haselmann et al., 2021).

The common conditioners are rolls and impellers. The stems are bent and broken by the rolls and water evaporates more easily from the cracks in the epidermis of legume forages. The plant cuticle is destroyed by the friction of the impellers' rotating fingers, which dries out the crop stem faster for grassy forages (Borreani et al., 2018; Greenlees et al., 2000; Lomas et al., 2018; Turul & Bozbay, 2023). For crimping devices, different forms of roll teeth have different flattening effects. 'Roll with spiral rectangular section lugs' Roll with spiral rectangular section lugs (RSRSL) has good inter-engagement, good crimping bending and a backward conveying effect; it is most widely used (Stanisavljević et al., 2021; Shinners et al., 2006; Hecker et al., 2022). To achieve flattening and crushing, the roll clearance needs to be less than the stem diameter. The drying velocity is increased by reducing the roll clearance and the effect is most obvious when the clearance is less than 2 mm (Shinners et al., 2006; Zhao et al., 2014; Tian et al., 2021; Li et al., 2021; Chen et al., 2015). The pressure of the conditioning roll on the alfalfa is controlled in the range 120-157 N, which helps to improve the drying efficiency (Zhang et al., 2020). The common materials used for the rolls are steel and urethane. Steel has better abrasion resistance than urethane and ti-core rolls but urethane has a better flattening effect and a lower crushed grass loss rate (Shinners et al., 2006; Rotz, 1995). Some scholars have proved, through experiments, that the faster the roll rotation velocity, the faster the conveying rate. On the contrary, as the flattening rate decreases, the crushed grass loss rate increases, resulting in harvest losses (Zhao et al., 2014; Wu et al., 2019; Wu et al., 2017).

[1] College of Mechanical and Electrical Engineering, Hunan Agricultural University, Changsha, China.
[2] Hunan Key Laboratory of Intelligent Agricultural Machinery and Equipment, Changsha, China.

Area Editor: João Paulo Arantes Rodrigues da Cunha
Received in: 3-15-2024
Accepted in: 3-13-2025

It has been shown that, in addition to the mechanical factors mentioned above, the airflow field in the cutting area of the mower has a non-negligible effect on the quality of forage harvesting. The airflow field in the cutting area is mainly formed by the high-velocity rotation of the cutter and the conditioning roll. At present, lawnmowers are the focus of research on the airflow field of cutters. Through Computational Fluid Dynamics (CFD) and other techniques, scholars have investigated the distribution of airflow (Xie et al., 2020; Wu et al., 2015; Kim & Kim, 2015; Kuriyagawa et al., 2021) and air pressure (Khodke et al., 2018; Ramnani et al., 2020) inside lawnmowers, to investigate the effects of blade speed (Edík et al., 2017) and blade geometry (Bhateja et al., 2020) on the airflow. Furthermore, the structural parameters of the cutter are optimised to determine the optimal parameters of the airflow field (Cedík et al., 2016; Wu et al., 2023). There are not many existing studies on the airflow field of the mower conditioner. In our team's previous research, the airflow field of the cutter of the mower conditioner was investigated and optimised by using a numerical simulation method (Jiang & Jiang, 2000). The high-velocity rotation of the rolls also disturbs the air, changing the airflow field, and the characteristics of the airflow field are affected by the structural parameters of the conditioning rolls. However, it is not clear how the structural and operational parameters of the conditioning rolls affect the airflow field around them.

Therefore, in this study, six different structural types of conditioning rolls were selected and the airflow field around the conditioning rolls was numerically simulated. Full factorial tests were carried out using CFD technology, using the roll clearance and the roll rotation velocity as the test factors. This testing studied the influence of structural and operational parameters, such as roll type, roll rotation velocity, and roll clearance, on the distribution of the airflow field around the conditioning roll and airflow velocity, to provide a reference basis for the optimised design of the conditioning roll of high-efficiency and low-loss forage harvesting equipment.

ROLL STRUCTURE AND AIRFLOW FIELD THEORY

Structure of conditioning roll

The operational area of the mower conditioner mainly consists of the cutter, conditioning rolls, frame, and other components (Figure 1). The conditioning rolls are mounted above the back of the cutter to flatten and condition the cut forage. To investigate the effect of roll type on the airflow field around the conditioning roll, six different types of conditioning rolls were designed in this study, based on Shinners et al. (2006), i.e. 'Roll with spiral rectangular section lugs' (RSRSL), 'Roll with triangular section lugs' (RTSL), 'Roll without lugs' (RWOL), 'Roll with circular section lugs' (RCSL), 'Roll with involute section lugs' (RISL), and 'Roll with rectangular section lugs' (RRSL). The structural parameters of each conditioning roll are shown in Figure 2 and Table 1.

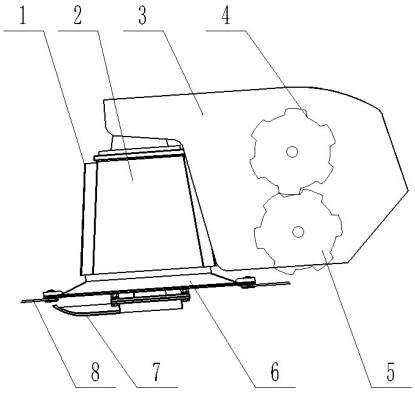

1. Guide plates 2. Conical drum 3. Side plate 4. Upper roll 5. Underlying roll 6. Tilting disc 7. Runner 8. Cutter

FIGURE 1. Structure of cutter and conditioner system.

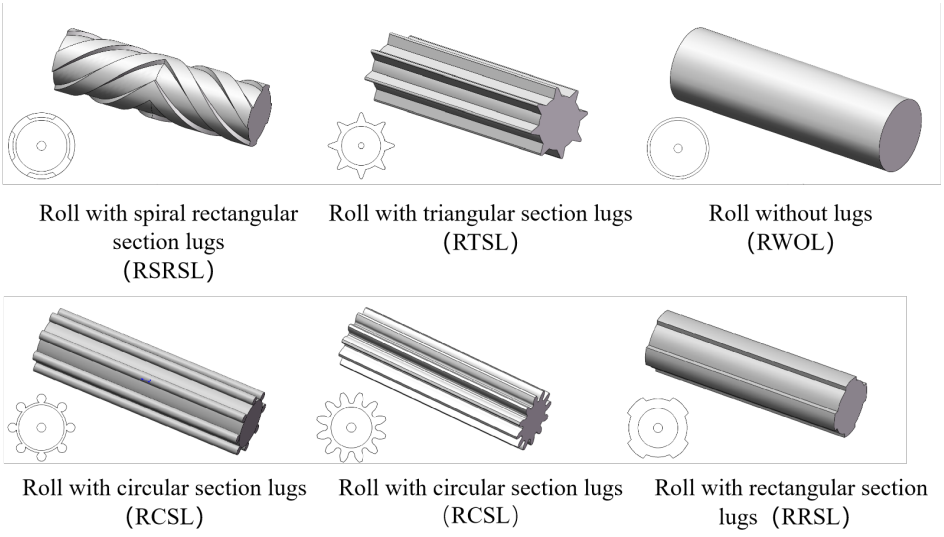

FIGURE 2. Types of conditioning roll.

TABLE 1. Structural parameters of roll.

Conditioner type	RSRSL	RTSL	RWOL	RCSL	RISL	RRSL
Cross-section shape of lugs	Rectangle	Triangle	-	Circle	Involute	Rectangle
Lug depth (mm)	1.3	3.8	0	3.8	2.9	2.5
Number of lugs	4	8	0	8	12	4
Lug pattern	Helical	Straight	Straight	Straight	Straight	Straight
Outer diameter (mm)	220	220	220	220	220	220
Roll length (mm)	730	730	730	730	730	730

Theoretical analysis of airflow field

The airflow field around the conditioning rolls is formed by the rolls rotating and disturbing the air. In our previous study of the cutter airflow field, the analytical method assumed that the single drum was a cylinder and the flow field around it was approximately regarded as a pure circulating flow (Wu et al., 2023; Jiang & Jiang, 2000). For a single conditioning roll rotation, the magnitude of the velocity v of the fluid microcluster at any point around it can be approximated as being inversely proportional to its polar radius r to the centre of rotation. Therefore, it can be expressed as follows:

$$v = \frac{c}{r} \tag{1}$$

Where:

c is a constant.

The velocity v could be decomposed along the X and Y directions as follows:

$$\begin{cases} v_x = -\frac{c}{r}\sin\theta = -\frac{cy}{x^2+y^2} \\ v_y = \frac{c}{r}\cos\theta = \frac{cx}{x^2+y^2} \end{cases} \tag{2}$$

Where:

θ is the angle between the line from the fluid microcluster to the centre of rotation and the x-direction.

By substituting the above equation into the fluid continuity equation, the following can be obtained:

$$\frac{\partial v_x}{\partial x} + \frac{\partial v_y}{\partial y} = \frac{\partial}{\partial x}\left(-\frac{cy}{x^2+y^2}\right) + \frac{\partial}{\partial y}\left(\frac{cx}{x^2+y^2}\right) = c \cdot \frac{0}{\left(x^2+y^2\right)^2} \tag{3}$$

It is known that the air flow around a single conditioning roll complies with the condition of continuous flow. For a single fluid microcluster, the angular velocity is expressed as follows:

$$\omega = \frac{1}{2}\left(\frac{\partial v_y}{\partial x} - \frac{\partial v_x}{\partial y}\right) = \frac{1}{2}\left[\frac{\partial}{\partial x}\left(\frac{cx}{x^2+y^2}\right) - \frac{\partial}{\partial y}\left(-\frac{cy}{x^2+y^2}\right)\right] = \frac{c}{2} \cdot \frac{0}{\left(x^2+y^2\right)^2} = 0 \tag{4}$$

Obviously, the air flow is an irrotational flow. In pure circulation flow, the velocity loop quantity of any curve enclosing the origin is constant and its magnitude is expressed as follows:

$$\Gamma = \int_L v \cdot ds = \int_0^{2\pi} \frac{c}{r} \cdot r \cdot d\theta = 2\pi c \tag{5}$$

The flow function ψ (x, y), which can be derived from the above equation, is expressed as follows:

$$d\psi = v_x dy - v_y dx = \frac{\Gamma}{2\pi}\left(-\frac{y}{x^2+y^2}\right)dy - \frac{\Gamma}{2\pi}\left(-\frac{x}{x^2+y^2}\right)dx = -\frac{\Gamma}{2\pi} \cdot \frac{dx^2+dy^2}{x^2+y^2} \tag{6}$$

To integrate it, the flow function can be expressed as:

$$\psi = -\frac{\Gamma}{4\pi}\ln\left(x^2+y^2\right) = -\frac{\Gamma}{2\pi}\cdot\ln\sqrt{x^2+y^2} = -\frac{\Gamma}{2\pi}\ln r \tag{7}$$

For the velocity potential function φ(x, y):

$$d\varphi = v_x dx + v_y dy = \frac{\Gamma}{2\pi}\left(-\frac{y}{x^2+y^2}\right)dx + \frac{\Gamma}{2\pi}\left(\frac{x}{x^2+y^2}\right)dy = \frac{\Gamma}{2\pi}\cdot\frac{xdy-ydx}{x^2+y^2} = \frac{\Gamma}{2\pi}\cdot\frac{d\left(\frac{y}{x}\right)}{1+\left(\frac{y}{x}\right)^2} \tag{8}$$

By integrating it, the velocity potential function can be expressed as:

$$\varphi = \frac{\Gamma}{2\pi}\arctan\frac{y}{x} = \frac{\Gamma}{2\pi}\theta \tag{9}$$

From eqs. (7) and (9), the flow function line of the airflow field around a single conditioning roll is a set of concentric circles centred on the rotation axis of the roll, while the isopotential line is a half a ray from the centre. This theory could provide a basis and reference for analysing the airflow field around a single roll. However, the airflow field around the roll is affected by various factors, including the shape of the rolls with lugs and roll position in practice, while the distribution and parameters of the airflow field tend to be inconsistent with the results of the theoretical analysis. For the intermeshing double rolls, the two streams of airflow intersect and collide in front of the conditioner, forming a relatively complex flow field. Consequently, it is difficult to build a theoretical model. Therefore, in this study, the CFD technique was applied to numerically simulate the airflow field around the intermeshing double rolls for analysis.

MATERIAL AND METHODS

Numerical simulation

According to our description in the literature (Wu et al., 2023), the immersed solid calculation method of CFX is used in this paper, to numerically simulate the airflow field around the conditioning roll. Firstly, the geometry of the roll was modelled using Solidworks software. Secondly, it was imported into the ICEM software after meshing. Thirdly, the physical model was defined by the CFX-Pre module and, finally, the numerical solution was obtained through the CFX-Solver module. The simulation results were visualised and data were extracted and analyzed with the CFX-Post module.

In this study, geometrical models of the conditioning roll and the fluid domain were created. When performing numerical simulations, the shape and size of the fluid domains of the single roll and the intermeshing double rolls were different. For the single roll simulation, the fluid domain was built as a cylinder with a diameter of 800 mm and a length of 2000 mm. When the intermeshing double roll simulation was performed, the fluid domain was built as a rectangle with a length of 2000 mm, a width of 1000 mm and a height of 1000 mm. For the simulation, the solid domain of the conditioning roll was placed at the centre of its fluid domain. For meshing, Tera/Mixed was selected as the mesh type and the tetrahedral mesh was created by Robust (Octree). When the solid domain mesh of the conditioning roll was created, the control global mesh size factor was defined with a scale factor of 1 and a maximum element value of 3, so its maximum allowed mesh size was 3 mm. When the fluid domain mesh was created, the control global mesh size factor was set to a scale factor of 1 and the maximum element value was 15; this allowed a maximum mesh size of 15 mm. The physical model was defined and the solution parameters were set by CFX-Pre. Air at 25 °C was chosen as the fluid material, the k-epsilon turbulence model was chosen for the computational model. The boundary condition of the fluid domain was set as OPENING in the software, for the simulation of the free-flow air around the rolls. The boundary condition of the solid domain was set as WALL. For the solid domain of rolls, Immersed Solid was selected as its type, and the rotating motion was selected. For the solution, transient simulation was used as the type of analysis, with a total simulation time of 2 s and a simulation step selected as 0.05 s.

Experimental factors and levels

In this study, the airflow field analysis was separately carried out for a single roll and double rolls. For the simulation of a single roll, the type and velocity of conditioning rolls were selected as the evaluation factors. For the simulation of intermeshing double rolls, roll type, roll rotational velocity, and roll clearance were selected as the experimental parameters. For the test, six types of conditioning roller were selected, as described in Figure 2. For the rotational velocity of the conditioning roll, its circumferential velocity was often 3.5-4.0 times the machine's forward velocity. The roll velocity of the mower conditioner used in this paper was 7-9 m/s. For the roll clearance, too-small a gap could easily cause material congestion, while too-large a clearance would reduce the alfalfa flattening rate. In the reference (Shinners et al. 2006), the roll clearance was set to three levels: 1, 3, and 5 mm. In summary, the table of test factor levels is presented in Table 2 and the full factorial simulation test was conducted based on the above factor levels.

TABLE 2. Factors and levels

Level	Factor		
	Roll Type	Roll Velocity *n* (r/min)	Roll Clearance *m* (mm)
1	RSRSL	400	1
2	RTSL	500	3
3	RWOL	600	5
4	RCSL	700	
5	RISL	800	
6	RRSL		

Evaluation Indexes

In order to quantitatively assess the effect of the parameters of the conditioning roll on the airflow field, the average velocity of the airflow around the roll was used as a test index when simulating the airflow field of a single roll. At the same time, in order to summarise the distribution rule of airflow velocity around the roll, the velocity at different distances from the centre of the roll was counted in the test. In the simulation of the airflow field of intermeshing double rolls, the velocity of the back-feeding airflow was used as a test index because the back-feeding airflow has a great impact on the working performance of the mower conditioner. The direction of the back-feeding airflow is opposite to the direction in which the forage is fed into the mower. Excessive back-feeding airflow can prevent forage from being fed to the rolls, so that the cutter in front of the rolls will keep re-cutting the forage, resulting in forage breakage (Wu, 2017).

Through the CFX-Post module, four lines of equal length to the conditioning roll (L_1, L_2, L_3 and L_4) (Figure 1) were established in the four vertical directions around the roll, at a position 120 mm from the roll centreline, with 60 measurement points evenly distributed on each of the four lines. The air velocity in the direction of roll rotation at each measurement point was exported by the software and the data at 240 measurement points were obtained.

The average velocity of airflow around the flattening roller was calculated as follows:

$$V_1 = \frac{\sum_{i=1}^{n}\left(V_{1i} + V_{2i} + V_{3i} + V_{4i}\right)}{4a} \quad (10)$$

in which:

V_{1i} - the X-direction airflow velocity at the *i*th measurement point on L_1, in m/s;

V_{2i} - the -Z-direction airflow velocity at the *i*th measurement point on L_2, in m/s;

V_{3i} - the -X-direction airflow velocity at the *i*th measurement point on L_3, in m/s;

V_{4i} - the Z-direction airflow velocity at the *i*th measurement point on L_4, in m/s;

a - the number of measurement points in each line segment, $a = 60$.

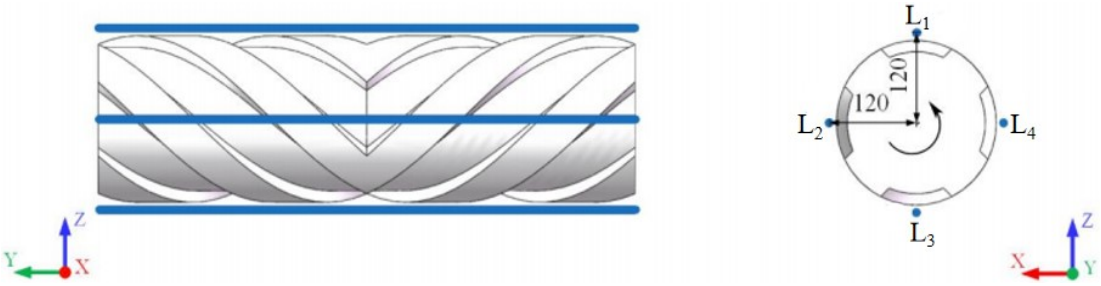

FIGURE 3. Measuring positions of the airflow velocity.

In the four radial directions of the roll, at 120-330 mm from the roll axis (Figure 4), each direction was equally spaced to establish 8 line segments equal to the length of the roll. The four directions of the line segments were L_{1j}, L_{2j}, L_{3j} and L_{4j}, with each line segment being evenly distributed on the 60 measurement points. The air velocity at each measurement point, in the same direction of roll rotation, was exported by the software and the data at 240 measurement points were obtained.

The average velocity of the airflow at each position in the radial direction of the conditioning roll was calculated as follows:

$$V_j = \frac{\sum_{i=1}^{n}\left(V_{1ji} + V_{2ji} + V_{3ji} + V_{4ji}\right)}{4a} \quad (11)$$

in which:

V_j - the average velocity of the airflow at each distance of the radial position of the roll, in m/s, j=1,2,3,4,5,6,7,8;

V_{1ji} - the X-direction airflow velocity at the *i*th measurement point on L_{1j}, in m/s;

V_{2ji} - the -Z-direction airflow velocity at the *i*th measurement point on L_{2j}, in m/s;

V_{3ji} - the -X-direction airflow velocity at the *i*th measurement point on L_{3j}, in m/s;

V_{4ji} - the Z-direction airflow velocity at the *i*th measurement point on L_{4j}, in m/s;

a - the number of measurement points in each line segment, $a = 60$.

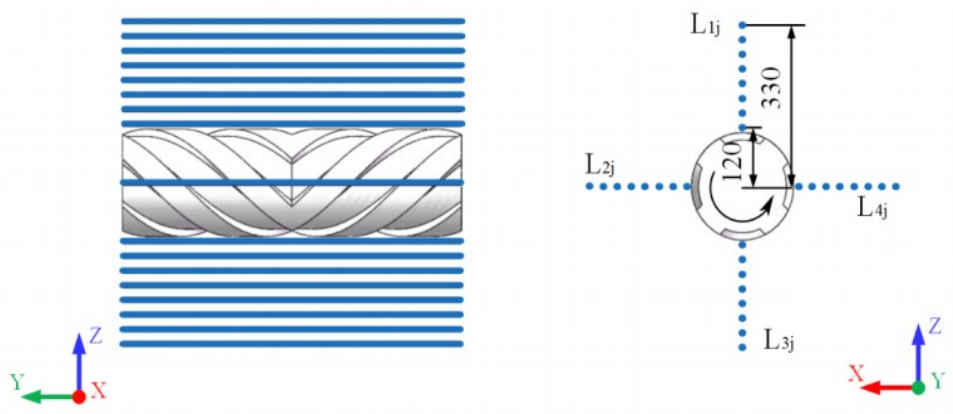

FIGURE 4. Measuring positions of distribution location

A line segment L_5 equal to the length of the rolls was created with 60 measurement points, evenly spaced across the segment at a position 290 mm (Figure 5) from the tangent point of the rolls and directly in front of the intermeshing double rolls. The airflow velocity at each measurement point was obtained in the same direction as the machine's forward direction (-Z-direction), resulting in airflow velocity data at 60 measurement points.

The back-feeding airflow velocity for intermeshing double rolls was calculated as follows:

$$V_2 = \frac{\sum_{i=1}^{n} V_{5i}}{a} \quad (12)$$

in which:

V_{5i} - the -Z-direction airflow velocity at the ith measurement point on L_5, in m/s;

a - the number of measurement points in each line segment, a = 60.

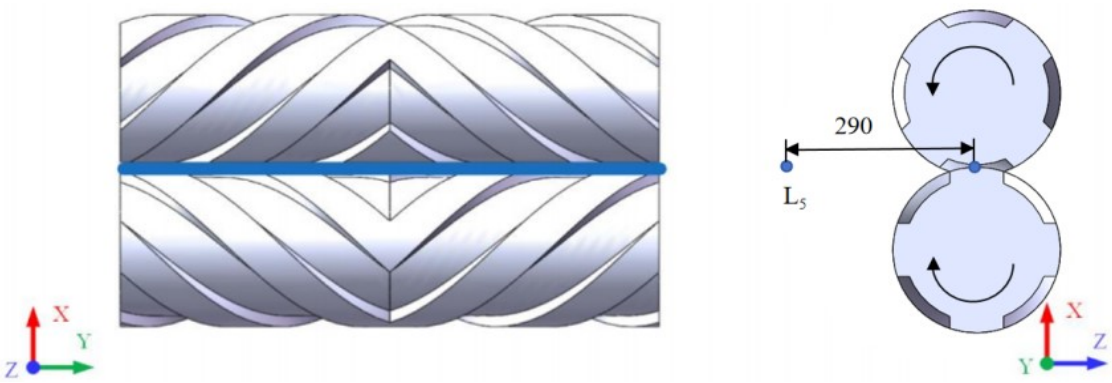

FIGURE 5. Measuring positions of back-feeding airflow velocity.

RESULTS AND DISCUSSION

Distribution of airflow field

When the roll rotation velocity was 600 r/min, the results of the airflow field distribution around the single roll were as shown in Figure 6.

Figure 6 shows that, with the rotation of the conditioning roll, the airflow around the roll is disturbed by the roll to form an airflow field in the same direction as the rotational velocity. When the roll's rotation velocity is certain, different types of rolls have different disturbing effects on the airflow, indicating that the shape and size of the lugs have a greater effect on the airflow field around the conditioning roll. According to the colour markings in the figure, it can be seen that the order of the size of the degree of air disturbance by the roll is in the order of RISL > RCSL > RSRSL > RRSL > RTSL > RWOL.

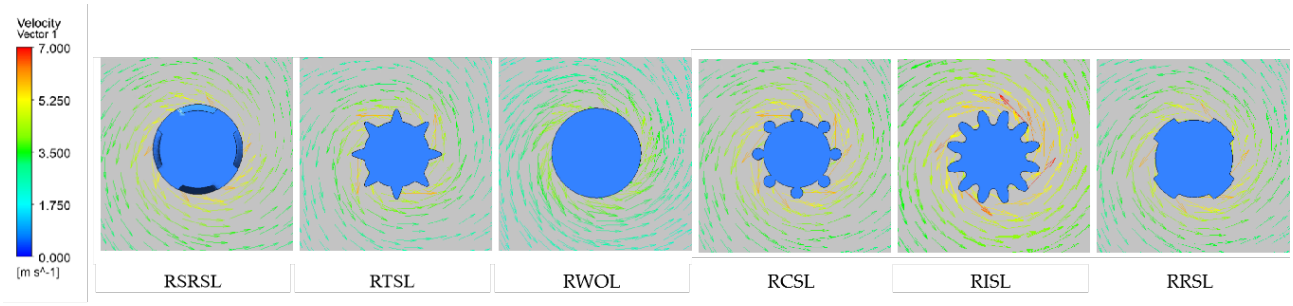

FIGURE 6. Distribution of airflow field around a single roll.

When the intermeshing double rolls' rotation velocity was 600 r/min and clearance was 3mm, the results of the airflow field distribution around the rolls were as shown in Figure 7. With the intermeshing double rolls rotating, the air is driven by the conditioning rolls to form an airflow intersection right in front of the rolls, resulting in a back-feeding airflow. The colour markings show that RTSL disturbed the air the least and there was no difference in the effect of air being disturbed by the other types of rolls.

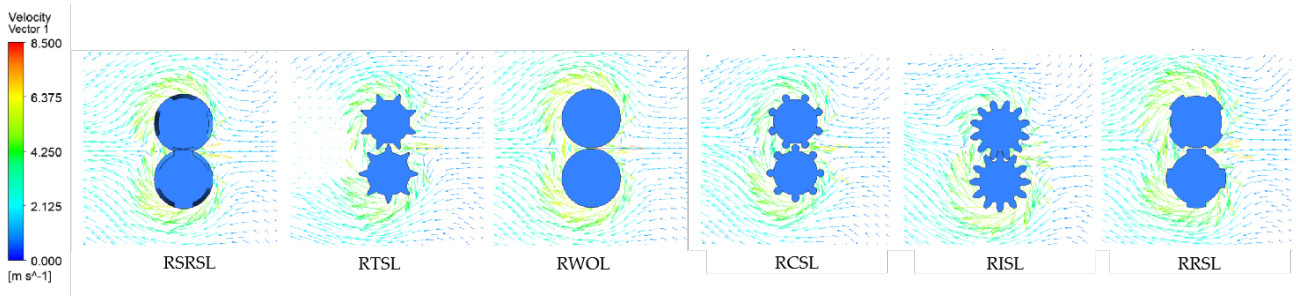

FIGURE 7. Distribution of airflow field around intermeshing double rolls.

Velocity of airflow

Velocity of airflow around a single roll

Figure 8 shows the velocity of the airflow around a single roll. The closer the colour of the graph is to red means that the airflow is faster; the closer to blue means that the airflow is slower. The colour markings show that the airflow velocity around the conditioning roll increases with increasing roll velocity, for each type of roll. In addition, the airflow around RTSL is the slowest and the airflow around RWOL and RISL is the fastest, when compared to the other roll types

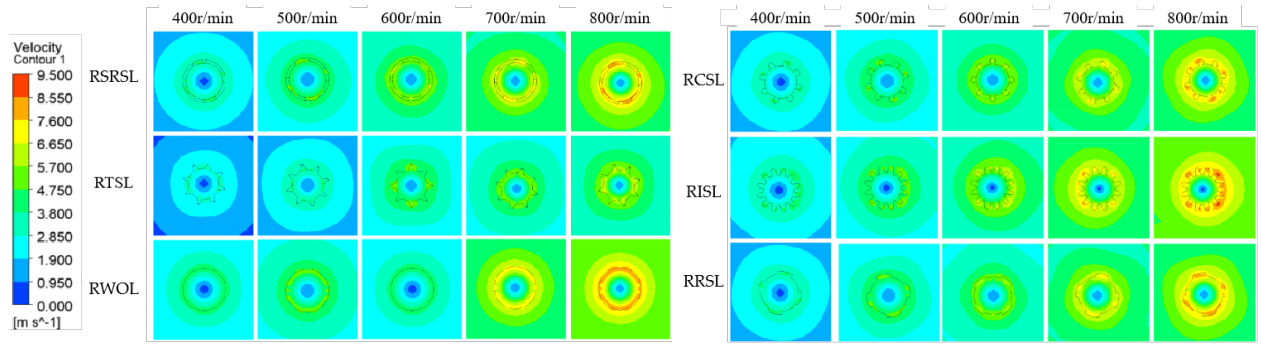

FIGURE 8. Velocity of airflow around a single roll.

The average airflow velocity around a single roll was processed according to the statistical method described in the preceding paragraphs and [eq. (10)]. As shown in Figure 9, when the rotational speed of the roll is increased from 400 to 800 r/min, the average velocity of the airflow around the roll shows a linear increasing trend, which conforms to the primary function for fitting.

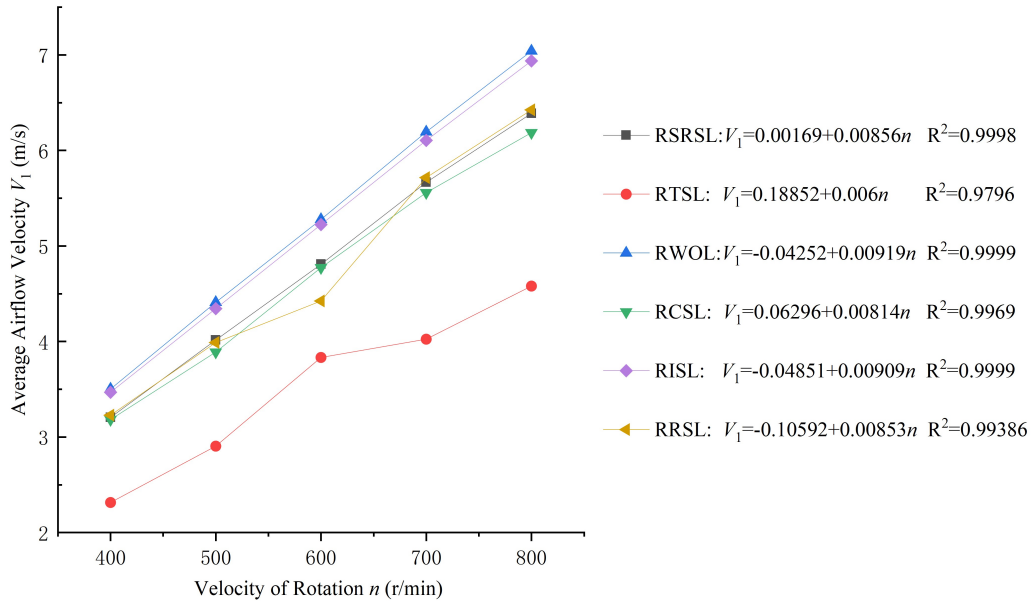

FIGURE 9. Average velocity of airflow around a single roll.

The average airflow velocity around a single roll was processed according to the statistical method in Section 3.3 and [eq. (11)]. When the velocity of the roll is 600 r/min, the average airflow velocity shows an exponentially decreasing trend, the farther away from the centre of the roll you go, which is in accordance with the image of the exponential function.

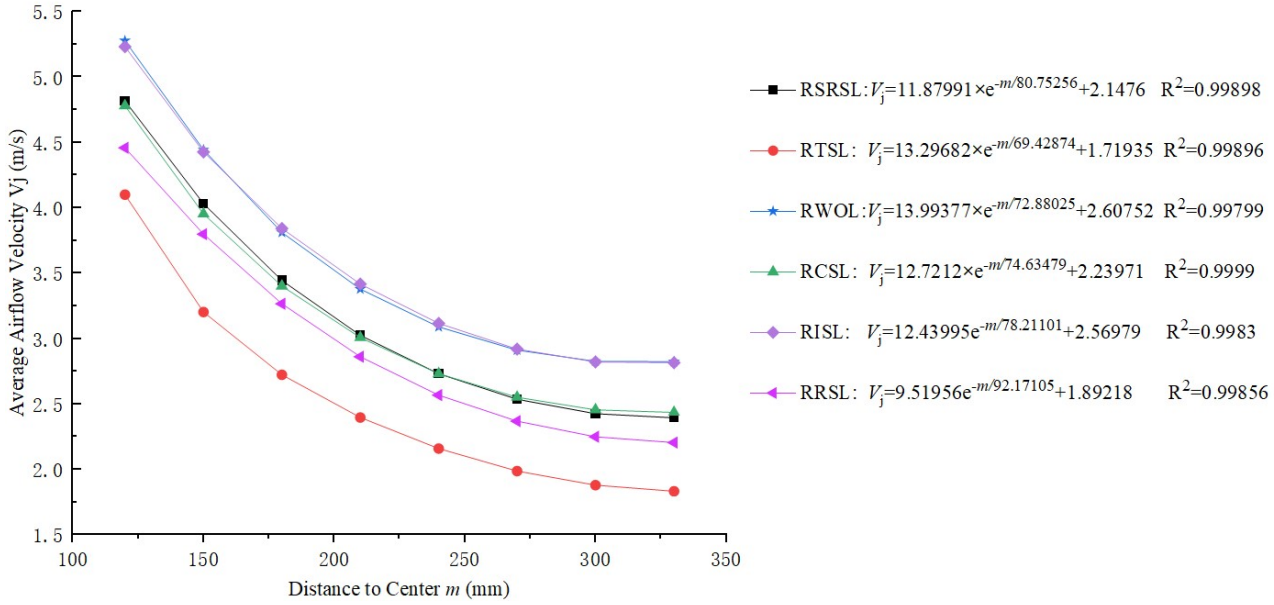

FIGURE 10. Average velocity of different distances of the rolls.

Velocity of airflow around the intermeshing double rolls

In Figure 11, when the velocity of intermeshing double rolls is 600 r/min and roll clearances are 3 mm, the airflow around RWOL is the fastest, while RISL is the slowest, as shown by the colour markings. The software indicated that the maximum air velocity around each type of roll is: RSRSL - 7.915 m/s, RTSL - 6.812 m/s, RWOL - 8.377 m/s, RCSL - 6.930 m/s, RISL - 6.511 m/s, and RRSL - 6.750 m/s.

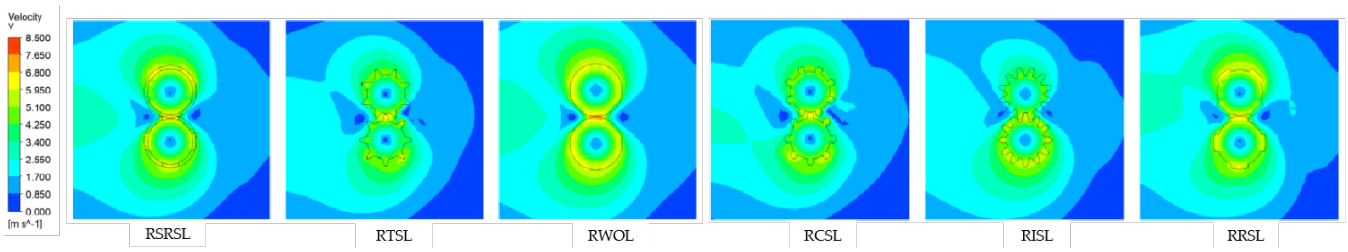

FIGURE 11. Velocity of the airflow around different types of rolls.

The RSRSL airflow velocities around the double rolls, with a 3 mm clearance and different rotational velocity, are shown in Figure 12. The figure shows that the airflow velocity increases with the increase in roll velocity. The maximum velocity of the airflow around the roll increased from 5.278 to 10.566 m/s when the roll velocity was increased from 400 to 800 r/min, using software statistics.

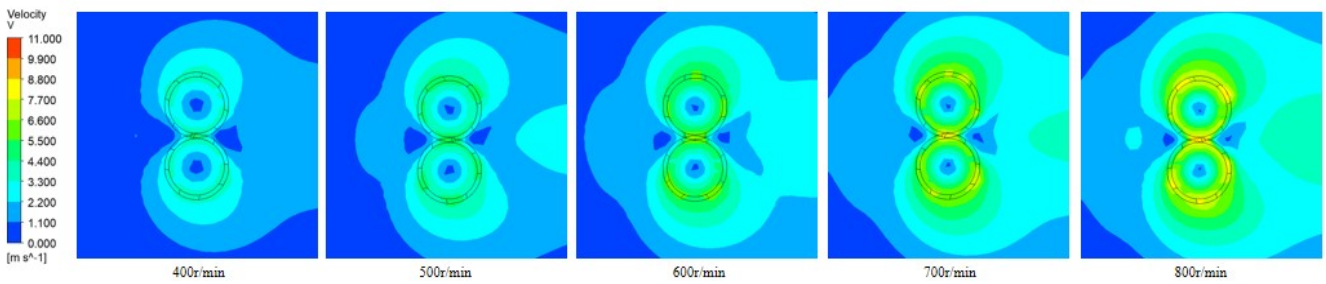

FIGURE 12. Velocity of the airflow around the double RSRSL.

Figure 13 shows the double RSRSL for the roll velocity of 600 r/min and different roll clearances. The result that the air velocity decreases as the roll clearance increases (but not by much) can be obtained from the graph. From the software, it can be seen that the roll clearance increased from 1 to 5 mm and the maximum airflow velocity around the roll decreased from 7.850 to 7.502 m/s.

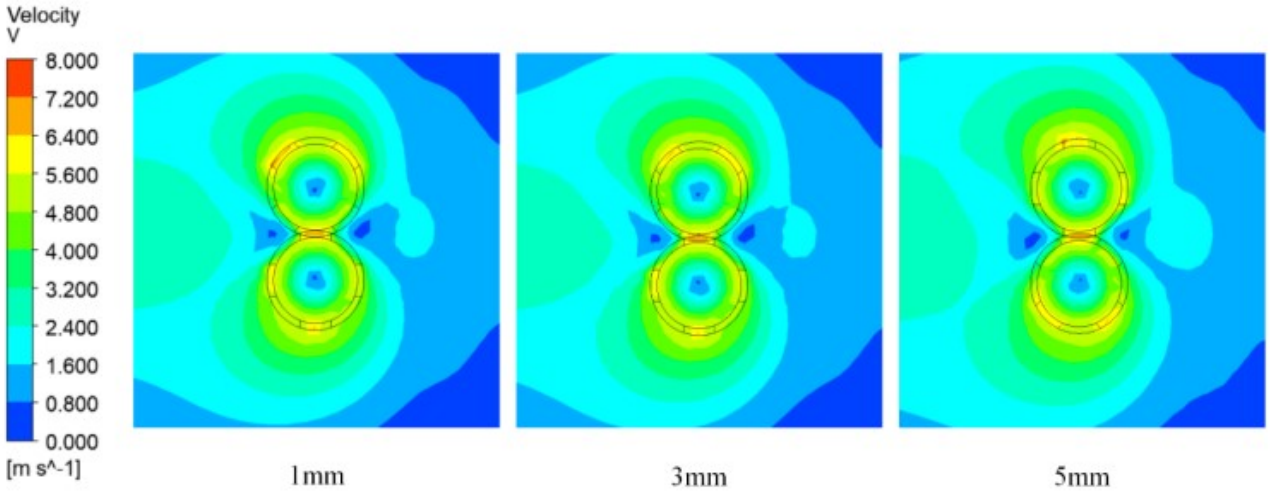

FIGURE 13. Airflow velocity around rolls with different clearances.

According to the statistical method described in Section 3.3 and [eq. (12)], for the velocity of the back-feeding airflow of the double rolls, the results are shown in Table 3 and Figure 14. When the mower condition is operating, less back-feeding airflow is required to make the alfalfa easier to feed. In order to better-predict the magnitude of the forward thrust airflow velocity, binary linear regression was performed to obtain the forward thrust airflow velocity prediction model (see Table 3 and Figure 14).

TABLE 3. Result of back-feeding airflow.

Rotation velocity (r/min)	Roll Clearance (mm)	RSRSL (m/s)	RTSL (m/s)	RWOL (m/s)	RWOL (m/s)	RISL (m/s)	RRSL (m/s)
400	1	1.6936	1.3717	1.4315	1.5258	1.2793	1.7637
400	3	1.6607	1.2018	1.6893	1.5116	1.2351	1.6824
400	5	1.4827	1.1593	1.6440	1.6009	1.4049	1.6118
500	1	2.0958	1.8478	1.7695	1.8696	1.5905	2.1047
500	3	2.0587	1.7954	2.0852	1.8549	1.5351	2.0615
500	5	1.8394	1.7496	2.0280	1.8878	1.7335	2.0022
600	1	2.5001	1.7699	2.1166	1.9755	1.9052	2.5660
600	3	2.4428	1.8220	2.4913	1.9859	1.8391	2.2619
600	5	3.1599	1.8081	2.4225	2.1423	2.0821	2.1904
700	1	2.9014	2.2705	2.4674	2.6332	2.2225	3.0393
700	3	2.8408	1.9801	2.9038	2.6013	2.1453	2.8935
700	5	2.5502	1.8967	2.8235	2.7356	2.4231	2.7662
800	1	3.3271	3.0172	2.8193	2.9860	2.5401	3.3124
800	3	3.2625	2.9111	3.3177	2.9601	2.4519	3.2680
800	5	2.9285	1.6244	3.2258	3.0015	2.7580	3.1834

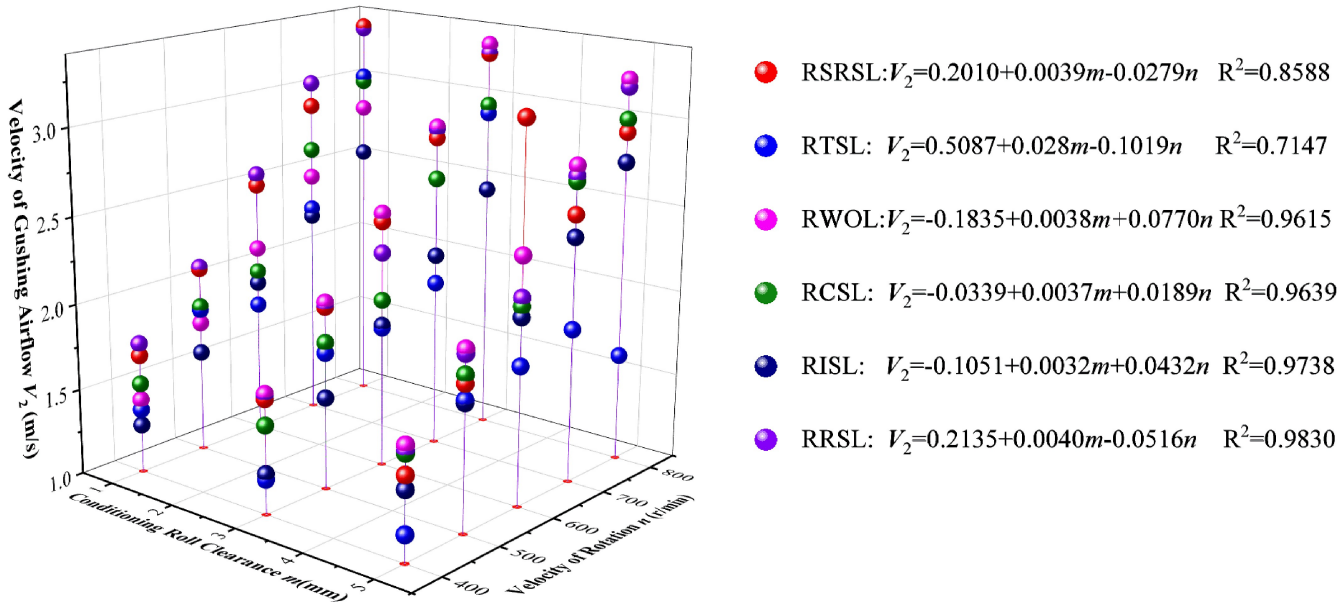

FIGURE 14. Velocity of back-feeding airflow and prediction model

VERIFICATION EXPERIMENTS

Test equipment

In order to verify the accuracy of the numerical simulation and the validity of the prediction model, conditioning roll test equipment was constructed and verification tests were carried out. As shown in Figure 15, the double rolls are driven by gear meshing and rotate relative to each other; the speed of the conditioning roll could be adjusted by the frequency converter. The test bench uses the most commonly used RSRSL on the mower conditioner. When testing with double rolls, the conditioning roll clearance is fixed at 5 mm. During the test, the air velocity of the airflow field was measured by using a hand-held thermal anemometer (TES-1341, TES Electrical Electronic Corp., air velocity range 0.3~30 m/s, resolution 0.01 m/s, measurement accuracy ±1%).

1. Shaft coupling 2. Motor 3. Frequency Converter 4. Frame 5. Conditioning roll 6. Gears.

FIGURE 15. Conditioner roll test device.

Test Methods

The airflow velocity tests for single and double rolls were performed at five conditioning roll velocity gradients (400, 500, 600, 700, and 800 r/min). In the double rolls airflow test, the roll clearance was 5 mm and the airflow velocity measurement method was consistent with the simulation test. For a single roll, the average velocity of the airflow around the roll was tested and double rolls tested the velocity of the back-feeding airflow. In the test, a TES-1341 thermal anemometer was utilised to automatically record a value every 2 s, at each measurement point, then the average value of each measurement point was read.

Test Results

The results of the validation tests and their comparison with the regression model predictions are shown in Table 4; the model predictions are calculated from eqs. (10) and (12), respectively.

TABLE 4. Validation test results.

Indexes	Roll Velocity (r/min)	Model Predicted Values (m/s)	Measured Value (m/s)	Error (%)	Average of Errors (%)
Average velocity of airflow around a single roll V_1	400	3.4012	3.187±0.078	6.72	6.35
	500	4.2352	4.021±0.067	5.33	
	600	5.0692	4.807±0.090	5.44	
	700	5.9032	5.516±0.082	7.01	
	800	6.7372	6.281±0.110	7.26	
Velocity of back-feeding airflow V_2	400	1.6215	1.446±0.037	6.68	5.86
	500	2.0115	1.818±0.035	7.57	
	600	2.4015	2.204±0.037	6.73	
	700	2.7915	2.451±0.121	5.34	
	800	3.1815	2.995±0.059	2.96	

From the test results, it can be seen that the average velocity of the airflow around a single roll and the velocity of back-feeding airflow both increase with an increase in the speed of the conditioning roll; the trend is consistent with the simulation test results. The results of the regression model, compared to the measured values of airflow velocity, show an average error of 6.35% for the predicted value of the average velocity of single roll airflow and 5.86% for the predicted value of the velocity of intermeshing double rolls' back-feeding airflow. The predicted values of the model match the measured values, which verify the accuracy of the numerical simulation and the validity of the predicted regression model.

CONCLUSIONS

In this study, based on the theoretical analysis of the airflow field, six different types of conditioning rolls were created and numerical simulation was then used to study the effects of conditioning roll type, roll velocity, and roll clearance on the airflow field around the conditioning roll. A regression model for predicting the airflow velocity around the roll was constructed and testing equipment was built to validate the results. The main conclusions of this paper are:

(1) The conditioning roll type had a significant effect on the airflow velocity around a single conditioning roll, with the fastest airflow velocity being identified around RWOL and RISL. The slowest airflow velocity was found around RTSL. The average airflow velocity around the conditioning roller had a linear positive correlation with the rotational velocity of the roll and an exponential negative correlation with the distance from the centre of the roll.

(2) When the intermeshing double rolls rotated in mutual meshing, the airflow around RWOL was the fastest, and RISL was the slowest. The airflow velocity around rolls increased with the increase in conditioning roll velocity and decreased with the increase in roll clearance.

(3) A regression prediction model was created for the average velocity of airflow around a single roll and the back-feeding airflow velocity of the intermeshing double rolls. Testing equipment was built to validate the airflow velocity. The results show that the average error of the regression model, with an average velocity of the airflow around a single roll, is 6.35%. The average error for the velocity of the back-feeding airflow in the intermeshing double rolls is 5.86%. The simulation results and prediction model were reliably confirmed and the results of the study could provide a reference for the optimised design of the conditioning roll.

ACKNOWLEDGEMENTS

This research was supported by the Hunan Provincial Natural Science Foundation of China (2024JJ5194), the Scientific Research Fund of the Hunan Provincial Education Department (23A0181), and Postgraduate Scientific Research Innovation Project of Hunan Province (CX20230723).

AUTHOR CONTRIBUTIONS

Conceptualization, Q.X., T.Z. and B.W.; methodology, Q.X. and B.W.; software, Q.X., B.W. and T.Z.; validation, Q.X., T.Z.; formal analysis, Q.X., H.Q. and B.W.; investigation, Q.X., B.W., T.Z. and T.H.; resources, B.W.; data curation, Q.X. and H.Q.; writing—original draft preparation, Q.X. and B.W.; writing—review and editing, B.W.; visualisation, B.W. and T.Z.; supervision, B.W.; project administration, B.W.; funding acquisition, B.W. All authors have read and agreed to the published version of the manuscript.

DATA AVAILABILITY STATEMENT

All data are presented in this article in the form of figures and tables.

CONFLICT OF INTEREST

The authors declare no conflict of interest.

REFERENCES

Bhateja, N., Sethi, N., Jain, S., & Mishra, Y. (2020). Lawn mower - An automated machine. *International Journal of Innovative Research in Computer Science & Technology (IJIRCST)*, *ISSN,* 2347-5552. https://doi.org/10.21276/ijircst.2020.8.6.7

Blain, G., Assuero, S. G., & Berone Germán D. (2023). Forage production and perennial root biomass in Lucerne under two cutting heights. *RIA. Revista de investigaciones agropecuarias,* 49(1), 15-22. https://doi.org/10.58149/s1hb-hw75

Borreani, G., Tabacco, E., Schmidt, R. J., Holmes, B.J., & Muck, R. A. (2018). Silage review: Factors affecting dry matter and quality losses in silages. *Journal of Dairy Science*, 101(5), 3952-3979. https://doi.org/10.3168/jds.2017-13837

Cedík, J., Pexa, M., Chyba, J., Vondrášek, Z., & Pražan, R. (2016). Influence of blade shape on mulcher blade air resistance. *Agronomy Research*, 14(2), 337–344. Available online: http://www.vuzt.cz/svt/vuzt/publ/P2016/018.pdf (accessed on 15 August 2022).

Chen, K., Zhao, C. H., Luo, Y. L., Ma, S. L., Bian, L. P., Zhou, Y., & Liu, J. Y. (2015). Design and test research of flattening gap adjustment device of mower conditioner. *Agricultural Research in the Arid Areas*, *33*: 278-282. https://doi.org/10.7606/j.issn.1000-7601.2015.03.44

Edík, J., Chyba, J., Pexa, M., Petrásek, S. (2017). Influence of shape of cutting tool on pressure conditions in workspace of mulcher with vertical axis of rotation. *Agronomy Research*, *15*, 1530-1539. https://doi.org/10.15159/AR.17.006

El-Baily, M. M. (2022). A study of rotary drum mower blade wear and its effects on forage productivity. *Poljopr Teh*, *47*(3), 87-100. https://doi.org/10.5937/PoljTeh2203087E

Feng, Y., Shi, Y., Zhao, M., Shen, H., Xu, L., Luo, Y., Liu, Y., Xing, A., Kang, J., Jing, H. (2022). Yield and quality properties of alfalfa (Medicago sativa L.) and their influencing factors in China. *European Journal of Agronomy*, *141*, 126637. https://doi.org/10.1016/j.eja.2022.126637

Greenlees, W. J., Hanna, H. M., Shinners, K, J., Marley, S. J., Bailey, T. B. (2000). A comparison of four mower conditioners on drying rate and leaf loss in alfalfa and grass. *Applied Engineering in Agriculture*, *16*(1). https://doi.org/10.13031/2013.4984

Haselmann, A., Kirchler, J., Fürst-Waltl, B., Zollitsch, W., Zebeli, Q., Knaus, W. (2021). The use of an impeller mowing conditioner during haymaking had no effects on feeding behavior, feed intake or performance of organic dairy cows. *Renewable Agriculture and Food Systems, 36*(6), 549-556. https://doi.org/10.1017/S1742170521000168

Hecker, L. P., Wätzold, F., Yang, X., Birkhofer, K. (2022). Squeeze it or leave it? An ecological-economic assessment of the impact of mower conditioners on arthropod populations in grassland. *Journal of Insect Conservation*, *26*(3), 463-475. https://doi.org/10.1007/s10841-022-00392-5

Jiang, E., & Jiang, Y. (2000). Studies on the characteristics of airflow field surrounding the stripping rotor with triangle plate teeth. *Nongye Gongcheng Xuebao (Transactions of the Chinese Society of Agricultural Engineering), 16*(1), 59-62. https://doi.org/10.13031/2013.9324

Kim, H. J., & Kim, S. H. (2015). A Study on Air Flow Characteristics of Mid-mower for Tractor (I). *Journal of the Korean Society of Manufacturing Process Engineers*, *14*(3), 27-35. https://doi.org/10.14775/ksmpe.2015.14..3.027

Khodke, K. R., Kukreja, H., Kotekar, S., Shende, C. J. (2018). Literature Review of Grass Cutter Machine. *Int. J. Emerg. Technol. Eng. Res*, *6*(2), 97-101.

Kuriyagawa, K., Yoshimura, H., & Tanabe, S. (2021). *U.S. Patent No. 11,109,532*. Washington, DC: U.S. Patent and Trademark Office.

Li, F. D., Xing, S. L., Tian, F. Y., Yan, Y. F., Wang, J., Song, Z. H. (2021). Design and Experiment of Toothed Roller Forage Crop Conditioning Test Bench. *Nongye Jixie Xuebao/Transactions of the Chinese Society of Agricultural Machinery*, *52*(6).

Li, F. F., Zhang, F. F., Wang, X. Z., Tang, K. T., Ma, C. H. (2019). Effects of cutting date and crop growth stage on alfalfa silage quality. *Acta Prataculturae Sinica*, *28*(12), 137-148.https://doi.org/10.11686/cyxb2019111

Liu, L. Y., Jia, Y. S., Fan, W. Q., Yin, Q., Cheng, Q. M., Wang, Z. J. (2022). An investigation of the main environmental factors affecting the natural drying of alfalfa for hay and hay quality. *Acta Prataculturae Sinica*, *31*(2), 121. https://doi.org/10.11686/cyxb2020529

Lomas, L. W., Slocombe, J. W., & Milliken, G. A. (2018). Storage losses from large round bales of alfalfa, tall fescue, and big bluestem hay. *Applied Engineering in Agriculture*, *34*(2), 445-454. https://doi.org/10.13031/aea.12681

Ramnani, S. M., Mekhe, B. R., Kuttamathu, A. B., Kotgire, S. S., Rajale, A.U. (2020). Unmanned automated lawn mower. *International Research Journal of Engineering and Technology (IRJET)*, *7*(6), 2473-2484.

Rotz, C. A. (1995). Field curing of forages. *Post-Harvest Physiology and Preservation of Forages*, *22*, 39-66, https://doi.org/10.2135/cssaspecpub22.c3

Shinners, K. J., Wuest, J. M., Cudoc, J. E., & Herzmann, M. E. (2006). Intensive conditioning of alfalfa: Drying rate and leaf loss. In *2006 ASAE Annual Meeting* (p. 1). American Society of Agricultural and Biological Engineers.

Stanisavljević, R., Vuković, A., Petrović, D. V., Radojević, R. L., Barać, S., Mileusnić, Z. (2021). Efficiency of alfalfa hay mowing machines under the dryland conditions. *Tehnički vjesnik*, *28*(5), 1503-1510. https://doi.org/10.17559/TV-20200720092823

Tian, F., Xia, K., Wang, J., Song, Z., Yan, Y., Li, F., & Wang, F. (2021). Design and experiment of self-propelled straw forage crop harvester. *Advances in Mechanical Engineering*, *13*(7). https://doi.org/10.1177/16878140211024455

Turul, K. M., Bozbay, C. K. (2023). Effect of two types of mowers on crop drying rate, yield and quality of alfalfa (medicago sativa l.). *Applied Ecologyand Environmental Research*, *21*(3), 2731-2745. https://doi.org/10.15666/aeer/2103_27312745

Wu, B., Wang, D., Wang, G., Fu, Z., & Guo, Z. (2015). Simulation analysis and experiment of profiling device of small self-propelled mower. *Transactions of the Chinese Society for Agricultural Machinery*, *46*(7), 123-129. https://doi.org/10.6041/j.issn.1000-1298.2015.07.019

Wu, B., Wang, D., Wang, G., Fu, Z., & Kang, C. (2017). Optimization and experiments of cut-condition device working parameter on mower conditioner. *Nongye Jixie Xuebao/Transactions of the Chinese Society of Agricultural Machinery*, *48*(10), 76-83. https://doi.org/10.6041/j.issn.1000-1298.2017.10.009

Wu, B., Wang, D., Wang, G., Kang, C., Ye, B., & Sun, Q. (2019). Experimental Study on Mechanical Properties of Connections between Alfalfa Leaves and Stems. In *2019 ASABE Annual International Meeting* (p. 1). American Society of Agricultural and Biological Engineers.

Wu, B., Zuo, T., Li, Z., Qian, H., Huang, T., & Xiang, Y. (2023). Numerical Simulation and Optimization of the Airflow Field of a Forage Drum Mower. *Applied Sciences*, 13(10), 5910. https://doi.org/10.3390/app13105910

Xie, S., Zhao, H., Yang, S., Xie, Q., & Yang, M. (2020). Design, analysis and test of small rotary lawn mower of single-disc type. *INMATEH-Agricultural Engineering*, *62*(3), 89-98. https://doi.org/10.35633/inmateh-62-09

Zhang, Q. F., Xie, H. X., Hu, Z. C., Zhong, B., Liu, Z. C. (2020). Design and experimental study of conditioning device for suspension silage machine. *Journal of Agricultural Mechanization Research*, *42*(10), 164-168. https://doi.org/10.13427/j.cnki.njyi.2020.10.028

Zhao, J., Guo, H., Wang, F., Zhang, X., Huang, S. (2014). Design and Test of Alfalfa Flattening Test Bench. *Transactions of the Chinese Society of Agricultural Engineering, 5*(45), 119-123. https://doi.org/10.6041/j.issn.1000-1298.2014.S0.020

Zhortuylov, O., Adilsheyev, A., Rzaliyev, A., Zhumatay, G., Bekenov, U., Zhortuylov, A. (2019). Mechanization of the haylage rolls wrapped with film on the basis of the modernization of drive of the mower-conditioner cutting machine. *EurAsian Journal of BioSciences, 13*(2), 749-756, https://www.proquest.com/scholarly-journals/mechanization-haylage-rolls-wrapped-with-film-on/docview/2259816419/se-2?accountid=45901